Journal of Applied Physics

Reducing interfacial thermal resistance between metal and dielectric materials by a metal interlayer

Cite as: J. Appl. Phys. 125, 045302 (2019); https://doi.org/10.1063/1.5079428
Submitted: 30 October 2018 . Accepted: 07 January 2019 . Published Online: 25 January 2019

Xiangyu Li, Wonjun Park, Yan Wang, Yong P. Chen, and Xiulin Ruan

View Online

Export Citation

CrossMark

ARTICLES YOU MAY BE INTERESTED IN

Phonon properties and thermal conductivity from first principles, lattice dynamics, and the Boltzmann transport equation
Journal of Applied Physics 125, 011101 (2019); https://doi.org/10.1063/1.5064602

Phonon thermal transport in encapsulated copper hybrids
Journal of Applied Physics 125, 045106 (2019); https://doi.org/10.1063/1.5082191

Nanoscale thermal transport. II. 2003–2012
Applied Physics Reviews 1, 011305 (2014); https://doi.org/10.1063/1.4832615

© 2019 Author(s).

Journal of Applied Physics ARTICLE scitation.org/journal/jap

Reducing interfacial thermal resistance between metal and dielectric materials by a metal interlayer

Cite as: J. Appl. Phys. **125**, 045302 (2019); doi: 10.1063/1.5079428
Submitted: 30 October 2018 · Accepted: 7 January 2019 ·
Published Online: 25 January 2019

View Online

Export Citation

CrossMark

Xiangyu Li,[1,2] Wonjun Park,[1,3] Yan Wang,[4] Yong P. Chen,[1,3,5] and Xiulin Ruan[1,2,a)]

AFFILIATIONS

[1] Birck Nanotechnology Center, Purdue University, West Lafayette, Indiana 47907, USA
[2] School of Mechanical Engineering, Purdue University, West Lafayette, Indiana 47907, USA
[3] School of Electrical and Computer Engineering, Purdue University, West Lafayette, Indiana 47907, USA
[4] School of Mechanical Engineering, University of Nevada, Reno, Nevada 89557, USA
[5] Department of Physics and Astronomy, Purdue University, West Lafayette, Indiana 47907, USA

[a)] Email: ruan@purdue.edu

ABSTRACT

Interfacial thermal resistance between metal and dielectric materials is a bottleneck of the thermal management for modern integrated circuits as interface density increases with thinner films. In this work, we have observed that the interfacial resistance across gold and aluminum oxide can be reduced from $4.8\times10^{-8}\,\mathrm{m^2\,K/W}$ to $1.4\times10^{-8}\,\mathrm{m^2\,K/W}$ after adding a nickel layer in between, which represents a 70% reduction. The two temperature model is applied to explain the reduction of interfacial resistance, and the results show that the nickel layer functions as a bridge that reduces the phonon mismatch between gold and aluminum oxide. Moreover, nickel has strong electron-phonon coupling, which reduces the thermal resistance caused by the weak electron-phonon coupling in gold.

Published under license by AIP Publishing. https://doi.org/10.1063/1.5079428

I. INTRODUCTION

As the thickness of thin films shrinks to micro/nano-scales, the interfacial resistance between metal and dielectric materials[1–5] ($\sim10^{-8}\,\mathrm{m^2\,K/W}$) becomes comparable to or dominant over the thermal resistance of thin films (~10 nm) in various engineering applications.[6–8] In these scenarios, interfacial thermal resistance has become a bottleneck for thermal management of nano-scale electronic devices. It is crucial to reduce such interfacial thermal resistances. For example, gold thin films have been widely used in electronic devices and the next generation data storage technology called heat-assisted magnetic recording (HAMR)[9–11] due to its high conductance, low loss, and chemical stability. The thin films are typically deposited on dielectric substrates which serve as heat sinks. Low interfacial thermal resistance and high thermal conductivity of the dielectric are desired for better thermal management. Unfortunately, the interfacial thermal resistance between gold and dielectric materials is still high. Reported results are around $2\times10^{-8}\,\mathrm{m^2\,K/W}$ when gold is deposited on the sapphire substrate.[2,12] However, when it comes to semiconductor devices, most aluminum oxide thin films for electrical insulation are amorphous.[13,14] The interfacial thermal resistance further increases to $1.1\times10^{-7}\,\mathrm{m^2\,K/W}$ if amorphous aluminum oxide is used.[15] English *et al.*[16] predicted, using molecular dynamics, that an intermediate layer to help bridge phonon spectra mismatch led to lower total resistance between metal and dielectric materials. Jeong *et al.*[17] inserted an interlayer of Cu and Cr between gold and sapphire substrates, reducing interfacial thermal resistance considerably, and they attributed the reduction to the bridging of phonon spectra mismatch. Recognizing that gold has weak electron-phonon coupling which introduces high electron-phonon non-equilibrium resistance, Wang *et al.*[18] proposed to insert a metal interlayer that has stronger electron-phonon

Published under license by AIP Publishing.

coupling to reduce this resistance. However, the possible role of electron-phonon coupling has not been evaluated in experiments. Also, such studies have not been done on amorphous aluminum oxide.

In this work, we have fabricated three layered structures on silicon substrates, consisting of gold, nickel, and aluminum oxide layers. The nickel layer was selected primarily because of its higher electron-phonon coupling factor. The interfacial thermal resistance characterization is done by the 3ω method. A 70% reduction of total interfacial resistance is observed after adding the nickel layer. The two-temperature model is used to explain the change of interfacial resistance, and the modeling results show similar trends with experimental data.

II. SAMPLE FABRICATION

Three structures, including reference sample A and two sandwich structures B and C, are fabricated to determine the interfacial thermal resistance between metal and aluminum oxide layers, as shown in Fig. 1 with TEM (Transmission Electron Microscope) images and schematic views. The silicon substrate is first cleaned with the RCA[19] (the Radio Corporation of America) method, and HF (Hydrogen Fluoride) is used to remove any oxidation layer and contaminations. This is crucial due to low thermal conductivity of silicon dioxide. Reference sample A has a 40 nm aluminum oxide layer on the silicon substrate. Sample B consists of a 20 nm aluminum oxide layer, 50 nm gold layer, and another 20 nm aluminum oxide layer on top, preserving the total thickness of the aluminum oxide layer. By splitting the aluminum oxide layer into two thinner ones, two gold-aluminum oxide interfaces are created for better measurement sensitivity, without introducing unwanted ones, such as gold-silicon interface. The surface also remains electrically insulating for the 3ω measurement. Sample C inserts 20 nm nickel layers in between the gold and aluminum oxide layers. The aluminum oxide layers are deposited with atomic layer deposition to ensure a consistent thickness, and metal layers are deposited by thermal evaporation. During FIB (Focused Ion Beam) lift-off for TEM images, a Pt layer is deposited on the surface to protect the sample during milling, which is still present in Fig. 1 as the unlabeled top layer above aluminum oxide.

III. INTERFACIAL THERMAL RESISTANCE CHARACTERIZATION

The differential 3ω method[20–22] is used to characterize the interfacial resistance in our work. It was developed to measure thin film thermal conductivity and interfacial resistance. In this work, a 30 μm wide and 3 mm long metal line is deposited using photolithography. Because of the small size of the metal line, the radiation loss even at high temperature is insignificant. With the joule heating of the metal line under AC current with frequency ω, the surface of the sample experiences a frequency-dependent temperature oscillation amplitude of $\Delta T(\omega)$, and the voltage has a frequency of 3ω. Detailed mathematic deviations can be found in the

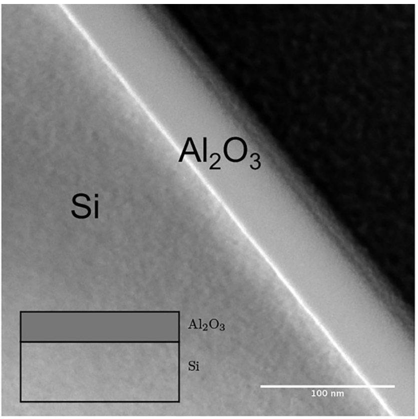

(a) Sample A

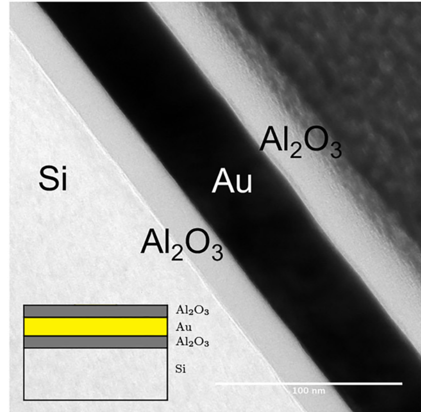

(b) Sample B

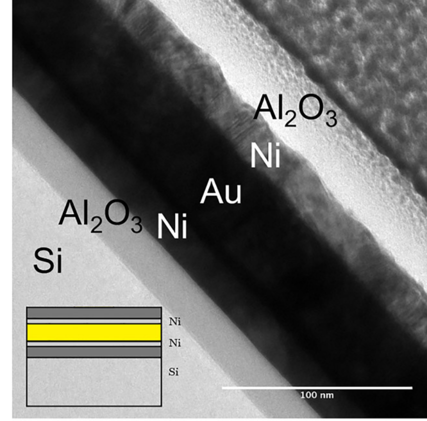

(c) Sample C

FIG. 1. Sandwich structures fabricated with multiple layers. (a) Sample A. (b) Sample B. (c) Sample C.

Published under license by AIP Publishing.

literature:[21,22]

$$\Delta T(\omega) = \frac{p}{2bl} R + C_o(\omega), \tag{1}$$

where p, b, and l are the power consumption, half width, and length of the metal line, repectively. C_o is dependent on frequency but remains the same across all three samples. R represents thermal resistance above the substrate. Thermal resistances of Ni and Au layers are neglected due to high thermal conductance and so is the interfacial resistance between them. The amorphous aluminum oxide thin films within 60 nm show similar thermal conductivity, reported by DeCoster *et al.*[23] Thus, the thermal resistance of aluminum oxide films is the same across all samples. The thermal resistance above the silicon substrate for each sample is

$$R_A = 2R_{Al_2O_3} + R_{Si-Al_2O_3}, \tag{2}$$

$$R_B = 2R_{Al_2O_3} + R_{Si-Al_2O_3} + 2R_{Au-Al_2O_3}, \tag{3}$$

$$R_C = 2R_{Al_2O_3} + R_{Si-Al_2O_3} + 2R_{Ni-Al_2O_3} + R_{Au-Ni}. \tag{4}$$

Subtracting reference sample A from samples B and C, we can associate thermal resistance difference ΔR_1 and ΔR_2 with $\Delta T(\omega)$ from the 3ω measurement, as shown below,[20]

$$\begin{aligned}\Delta R_1 &= R_B - R_A = 2R_{Au-Al_2O_3} \\ &= 2bl\left[\left(\frac{\Delta T(\omega)}{p}\right)_B - \left(\frac{\Delta T(\omega)}{p}\right)_A\right],\end{aligned} \tag{5}$$

$$\begin{aligned}\Delta R_2 &= 2R_{Ni-Al_2O_3} + 2R_{Au-Ni} \approx 2R_{Ni-Al_2O_3} \\ &= 2bl\left[\left(\frac{\Delta T(\omega)}{p}\right)_C - \left(\frac{\Delta T(\omega)}{p}\right)_A\right],\end{aligned} \tag{6}$$

where $\Delta T(\omega)$ from the 3ω measurement regarding to different samples as well as various frequencies are shown in Fig. 2. Sample B has an overall higher $(\Delta T/p)$, representing higher total resistance than Sample A due to the added Au layer. Sample C sits between Samples A and B, indicating total resistance is lowered as the nickel interlayer is added. All three $(\Delta T/p)$ curves are relatively parallel to each other. The thermal resistance difference is calculated from the average of the gaps between the curves at different frequencies. We obtained that the interfacial resistance between gold and aluminum oxide is $4.8 \pm 0.5 \times 10^{-8}\ m^2\ K/W$, and that between the nickel and aluminum oxide is $1.4 \pm 0.1 \times 10^{-8}\ m^2\ K/W$. This indicates a 70% reduction of resistance after inserting the Ni layer. The uncertainties are evaluated based on the variation of these gaps at different frequencies in Eqs. (5) and (6). In this case, sample B yields an uncertainty around 11.5%, and sample C an uncertainty of 7.9%.

IV. THEORETICAL ESTIMATION ON INTERFACIAL RESISTANCE

Because our metal-dielectric system involves both electrons and phonons, the two-temperature model suits as the tool for interfacial resistance estimation,[24–29] assuming two different temperatures for phonons and electrons, respectively, in the metal side. Wang *et al.*[29] combined the two temperature model with molecular dynamics to illustrate the impact of the electron-phonon coupling effect. The overall interfacial resistance consists of a phonon-phonon component R_{pp}, an electron-phonon nonequilibrium component R_{ep}, as well as an electrical inelastic scattering component, R_{ei}, as shown in Fig. 3.[30] The third component R_{ei} is estimated around $3431 \times 10^{-9}\ m^2\ K/W$ for Au and $4.3 - 5.9 \times$

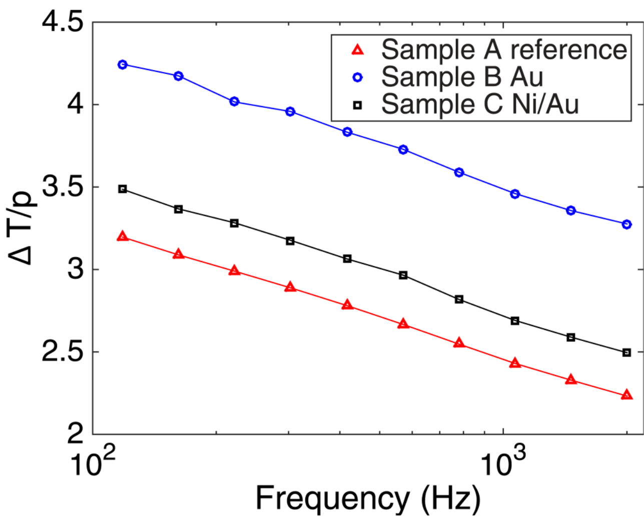

FIG. 2. 3ω measurement for three sandwich structures.

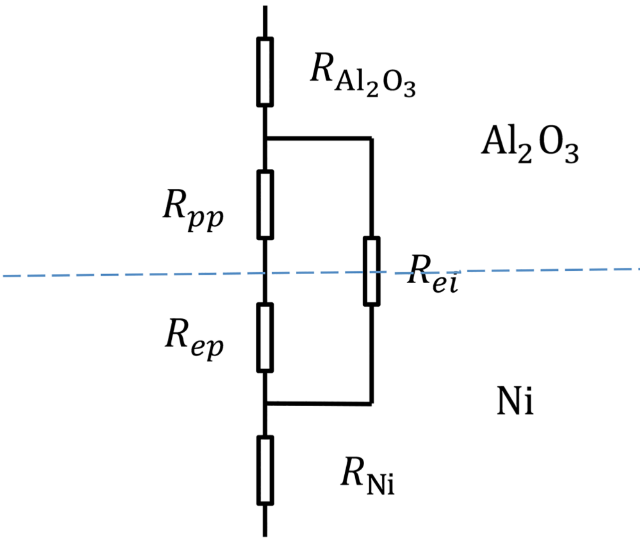

FIG. 3. Thermal resistance network between nickel and aluminum oxide.

Published under license by AIP Publishing.

10^{-9} m^2 K/W for Ni.[30–32] Thus, R_{ei} for Au will be neglected while that for Ni will be accounted.

The first part R_{pp} happens across both metal-dielectric and dielectric-dielectric interfaces. Acoustic mismatch model (AMM)[33,34] and diffuse mismatch model (DMM)[34] are two models widely used on different interface conditions. The former works mostly for ideal interfaces at low temperatures, which rarely happens in experiments. Hence, we use DMM here, which assumes phonons lose their correlations and randomize directions across the interface. We chose the [100] direction for Ni and Au, and [1010] for aluminum oxide for heat flux direction across the interface. The phonon density of states is shown for aluminum oxide, gold and nickel, respectively, in Fig. 4. To calculate phonon dispersion and density of states, we assume crystalline structures of metals and aluminum oxide layer for simplification. Since the metal layers are polycrystalline and an aluminum oxide layer is amorphous in our structures, the theoretical results would underestimate interfacial resistance. With film thicknesses higher than the phonon mean free path, the bulk phonon density of states is calculated for Au and Ni.[35] Amorphous alumina is reported with a different phonon density of states, though most of the differences are at frequencies over 10 THz, beyond the phonon frequency ranges of Ni and Au.[36] Please also note that our DMM and TTM results should be understood on a qualitative basis since they are intended for crystal alumina rather than amorphous alumina. In Fig. 4, both nickel and gold phonons overlap with aluminum oxide phonons at low frequencies where acoustic phonons dominate. Compared with gold, nickel phonons show a larger overlap with aluminum oxide, due

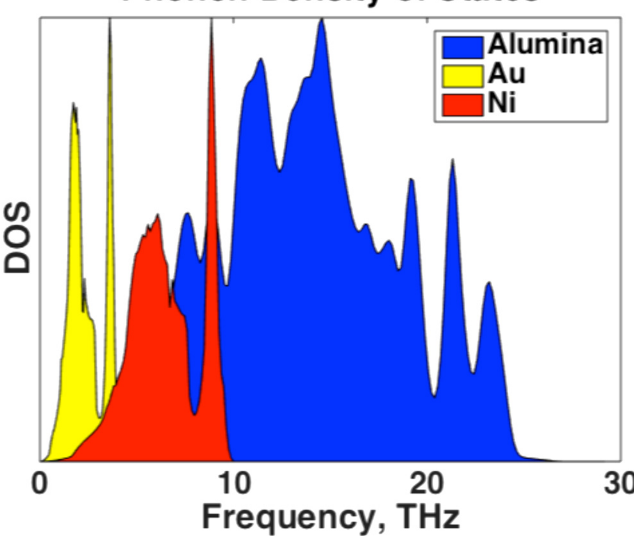

FIG. 4. Phonon density of states for Ni, Au, and aluminum oxide.

TABLE I. Properties for Ni and Au for R_{ei} calculation.

	γ (J m^{-3} K^{-2})	τ_{e-ph} (ps)	u_l (m/s)	u_t
Au	67.6[40]	3.1[41]	2131	1937
Ni	1077.4[42]	0.3-0.4[41]	5280	3643

to its smaller lattice constant and lighter atom mass, functioning as a phonon bridge between aluminum oxide and gold phonon frequencies. DOS can be affected by lattice constant, atom mass, and bonding strength, while a quantitative relation is rather complicated. For phonon transmission coefficient α, $\alpha_{A\to B} = \alpha_{B\to A}$ is satisfied. With that, R_{pp} can be calculated as[37]

$$h_{A\to B} = \frac{1}{2\pi A_c}\sum_j \int \hbar\omega M_A(\omega)\alpha_{A\to B}\frac{\partial f}{\partial T}d\omega, \tag{7}$$

$$\alpha_{A\to B}(\omega') = \frac{\sum_j M_B(\omega)}{\sum_j M_B(\omega) + \sum_j M_A(\omega)}, \tag{8}$$

$$M = \pi A_c\left(\frac{v_g}{2}\right)\frac{K(\omega)^2}{2\pi^2 v_g}, \tag{9}$$

where M is the number of phonon modes, j stands for phonon modes, A_c stands for contact region area, v_g is the group velocity, K is wavevector, and f is the Bose-Einstein distribution function. The results are shown in Table II.

For the resistance due to electron-phonon coupling, the two temperature model considers the electron-phonon coupling effect by assigning two temperatures for electrons and phonons. Since electrons are main carriers for heat transfer in most metals, the interfacial resistance based on the two-temperature model can be written as[24,29]

$$R_i = R_{ei}//(R_{pp}+R_{ep}) = R_{ei}//\left[\frac{1}{h_{pp}} + \left(\frac{k_e}{k_e+k_p}\right)^{3/2}\left(\frac{1}{G_{ep}k_p}\right)^{1/2}\right] \approx R_{ei}//\left[\frac{1}{h_{pp}} + \left(\frac{1}{G_{ep}k_p}\right)^{1/2}\right], \tag{10}$$

where G_{ep} is the electron-phonon coupling factor for metals,[26,38] k_e and k_p are the electron and lattice thermal conductivity of the metal, respectively, R_i is the overall interfacial thermal resistance, R_{pp} and h_{pp} are lattice mismatch resistance

TABLE II. Comparison between the TTM and 3ω measurement.

	R_{pp}[a]	R_{ep}[a]	R_i[a]	Experiment[a]
Au-Al_2O_3	20.6	4.3	24.9	48.4
Ni-Al_2O_3	6.7	0.2	2.9	14.0

[a]10^{-9} m^2 K/W.

Published under license by AIP Publishing.

and conductance, respectively, and R_{ep} is the interfacial resistance with regard to the electron-phonon coupling effect. G_{ep} is set as 2.88×10^{17} W/m^3 K for nickel and 2.6×10^{16} W/m^3 K for gold. $k_p = 18.5$ W/m K for 20 nm nickel film and $k_p = 1.5$ W/m K for 50 nm gold film from first principles calculations.[39]

We adopted the work of Sergeev[31] to estimate R_{ei}, the inelastic electron-boundary scattering in our system. The equation is as follows:

$$\sigma_K^{el} = \frac{3\pi\hbar}{35\zeta(3)k_B}\frac{\gamma u_l}{\tau_{e-ph}}\left[1 + 2\left(\frac{u_l}{u_t}\right)^3\right], \tag{11}$$

in which $\hbar$ is the reduced Planck constant, ζ is the Riemann Zeta function, k_B is the Boltzmann constant, γ is the Sommerfeld constant, τ_{e-ph} is the electron phonon relaxation time, and u is the sound velocity with the subscript l denoting longitudinal phonon and t for transverse waves. We used the properties listed in Table I in our calculation, where the group velocities are obtained from our own first-principles calculations.

We estimate the σ_K^{el} for Au-Al_2O_3 to be 291 397 W/m^2 K while that for Ni-Al_2O_3 to be $1.7 - 2.3 \times 10^8$ W/m^2 K. After converting these into resistances, we obtained $R_{ei,Au-Al_2O_3} = 3431 \times 10^{-9}$ m^2 K/W and $R_{ei,Ni-Al_2O_3} = 4.3 - 5.9 \times 10^{-9}$ m^2 K/W. The former one can be neglected, while the latter is included in the theoretical estimation in this revision.

In our study, theoretical estimations using the TTM are shown in Table II along with experimental data. It can be seen that inserting a Ni layer significantly reduces both R_{pp} and R_{ep}. With a Ni interlayer, R_{ep} almost diminishes, and R_{pp} dominates the overall interfacial resistance. Compared with gold, phonons in nickel show a larger match with those in aluminum oxide, resulting in lower phonon-phonon resistance than gold. The difference between experiments and theoretical estimations is mainly due to the fact that we used crystalline phonon properties for Al_2O_3. Adhesion between films is another significant factor leading to poor interfacial thermal resistance.[15,43,44] Lahmar *et al.* have measured interfacial thermal resistance of 1.1×10^{-7} m^2 K/W between gold and aluminum oxide, which decreases below 10^{-8} m^2 K/W after improving film adhesion by thermal treatment.[15] We also saw a rougher interface between nickel and aluminum oxide, which may have some effect on interfacial thermal resistance, but unlikely to be the major contribution. Despite these simplifications, our model reveals the same trends observed in experiments.

V. CONCLUSION

In this work, we measured the interfacial thermal resistance between gold and aluminum oxide before and after inserting a Ni interlayer. The interfacial resistance decreases by 70%, from 4.8×10^{-8} m^2 K/W to 1.4×10^{-8} m^2 K/W. Theoretical calculations using the diffuse mismatch model and two-temperature model show a similar trend with experimental data, indicating that the Ni layer significantly reduces both resistances due to phonon mismatch and electron-phonon non-equilibrium.

ACKNOWLEDGMENTS

Thanks go to Tianli Feng and Zexi Lu at Purdue University for their useful discussions in the two temperature model and phonon dispersion.

REFERENCES

[1] S.-M. Lee and D. G. Cahill, J. Appl. Phys. **81**, 2590 (1997).
[2] R. J. Stoner and H. J. Maris, Phys. Rev. B **48**, 16373 (1993).
[3] R. J. Stevens, A. N. Smith, and P. M. Norris, J. Heat Transfer **127**, 315 (2005).
[4] A. J. Griffin, F. R. Brotzen, and P. J. Loos, J. Appl. Phys. **75**, 3761 (1994).
[5] J. H. Kim, A. Feldman, and D. Novotny, J. Appl. Phys. **86**, 3959 (1999).
[6] B.A. Cola, J. Xu, C. Cheng, X. Xu, T. S. Fisher, and H. Hu, J. Appl. Phys. **101**, 1 (2007).
[7] C. Dames, J. Appl. Phys. **95**, 682 (2004).
[8] R. S. Prasher and P. E. Phelan, J. Heat Transfer **123**, 105 (2001).
[9] L. Pan and D. B. Bogy, Nat. Photonics **3**, 189 (2009).
[10] W. Challener, C. Peng, A. Itagi, D. Karns, W. Peng, Y. Peng, X. Yang, X. Zhu, N. Gokemeijer, Y.-T. Hsia *et al.*, Nat. Photonics **3**, 220 (2009).
[11] M. A. Seigler, W. A. Challener, E. Gage, N. Gokemeijer, G. Ju, B. Lu, K. Pelhos, C. Peng, R. E. Rottmayer, X. Yang *et al.*, IEEE Trans. Magn. **44**, 119 (2008).
[12] Y. Xu, H. Wang, Y. Tanaka, M. Shimono, and M. Yamazaki, Mater. Trans. **48**, 148 (2007).
[13] M. Specht, H. Reisinger, F. Hofmann, T. Schulz, E. Landgraf, R. Luyken, W. Rsner, M. Grieb, and L. Risch, Solid State Electron. **49**, 716 (2005), 5th International Workshop on the Ultimate Intergration of Silicon, ULIS 2004.
[14] P. Ye, B. Yang, K. Ng, J. Bude, G. Wilk, S. Halder, and J. Hwang, Appl. Phys. Lett. **86**, 063501 (2005).
[15] A. Lahmar, T. P. Nguyen, D. Sakami, S. Orain, Y. Scudeller, and F. Danes, Thin Solid Films **389**, 167 (2001).
[16] T. S. English, J. C. Duda, J. L. Smoyer, D. A. Jordan, P. M. Norris, and L. V. Zhigilei, Phys. Rev. B **85**, 035438 (2012).
[17] M. Jeong, J. P. Freedman, H. J. Liang, C.-M. Chow, V. M. Sokalski, J. A. Bain, and J. A. Malen, Phys. Rev. Appl. **5**, 014009 (2016).
[18] Y. Wang, Z. Lu, A. K. Roy, and X. Ruan, J. Appl. Phys. **119**, 065103 (2016).
[19] W. Kern and D. A. Puotinen, RCA Rev. **31**, 187 (1970).
[20] T. Borca-Tasciuc, A. R. Kumar, and G. Chen, Rev. Sci. Instrum. **72**, 2139 (2001).
[21] D. G. Cahill, Rev. Sci. Instrum. **61**, 802 (1990).
[22] D. G. Cahill, J. Vac. Sci. Technol. A **7**, 1259 (1989).
[23] M. E. DeCoster, K. E. Meyer, B. D. Piercy, J. T. Gaskins, B. F. Donovan, A. Giri, N. A. Strnad, D. M. Potrepka, A. A. Wilson, M. D. Losego, and P. E. Hopkins, Thin Solid Films **650**, 71 (2018).
[24] A. Majumdar and P. Reddy, Appl. Phys. Lett. **84**, 4768 (2004).
[25] D. M. Duffy and A. M. Rutherford, J. Phys. Condens. Matter **19**, 16207 (2007).
[26] Z. Lin, L. Zhigilei, and V. Celli, Phys. Rev. B **77**, 075133 (2008).
[27] L. Koči, E. M. Bringa, D. S. Ivanov, J. Hawreliak, J. McNaney, A. Higginbotham, L. V. Zhigilei, A. B. Belonoshko, B. A. Remington, and R. Ahuja, Phys. Rev. B **74**, 012101 (2006).
[28] R. E. Jones, J. A. Templeton, G. J. Wagner, D. Olmsted, and N. A. Modine, Int. J. Numer. Methods Eng. **83**, 940 (2010).
[29] Y. Wang, X. Ruan, and A. K. Roy, Phys. Rev. B **85**, 205311 (2012).
[30] Z. Li, S. Tan, E. Bozorg-Grayeli, T. Kodama, M. Asheghi, G. Delgado, M. Panzer, A. Pokrovsky, D. Wack, and K. E. Goodson, Nano Lett. **12**, 3121 (2012).
[31] A. Sergeev, Phys. Rev. B Condens. Matter Mater. Phys. **58**, R10199 (1998).
[32] A. Sergeev, Phys. B Condens. Matter **263–264**, 217 (1999).
[33] W. A. Little, Can. J. Phys. **37**, 334 (1959).
[34] E. Swartz and R. Pohl, Rev. Mod. Phys. **61**, 605 (1989).

Published under license by AIP Publishing.

[35] P. Heino and E. Ristolainen, Microelectronics J. **34**, 773 (2003).
[36] L. Chen, N. Kumari, and Y. Hou, AIP Adv. **7**, 115205 (2017).
[37] T. Fisher, *Thermal Energy at the Nanoscale*, Lessons from Nanoscience: A Lecture Notes Series Vol. 3 (World Scientific, 2013).
[38] C. L. Phillips and P. S. Crozier, J. Chem. Phys. **131**, 074701 (2009).
[39] Y. Wang, Z. Lu, and X. Ruan, J. Appl. Phys. **119**, 225109 (2016).
[40] J. Bearden and J. Thomsen, *American Institute of Physics Handbook* (McGraw-Hill, New York, 1972).
[41] M. van Kampen, J. T. Kohlhepp, W. J. M. de Jonge, B. Koopmans, and R. Coehoorn, J. Phys. Condens. Matter **17**, 6823 (2005).
[42] S. Link, C. Burda, Z. L. Wang, and M. A. El-Sayed, J. Chem. Phys. **111**, 1255 (1999).
[43] A. Lahmar, N. Hmina, Y. Scudeller, and J. Bardon, Thin Solid Films **325**, 156 (1998).
[44] T. P. Nguyen, J. Ip, P. Le Rendu, and A. Lahmar, Surf. Coatings Technol. **141**, 108 (2001).

Published under license by AIP Publishing.